ORIGINAL ARTICLE

Utilization of residual zinc–iron-layered double hydroxide after methyl orange management as a new sorbent for wastewater treatment

Doaa Moustafa[1] · Rehab Mahmoud[1,2] · Hanafy M. Abd El-Salam[2] · Nabila Shehata[1]

Abstract

In recent years, enormous attention has been attracted to layered double hydroxides (LDHs) due to their tunable chemical composition and physical properties. In this recent work, Zn–Fe LDH with nitrate as the interlayer anions was prepared via the co-precipitation technique. The production of Zn–Fe LDH was emphasized by different analyses like Fourier-transform infrared spectrometer (FT-IR), X-ray photoelectron spectroscopy (XPS), zeta potential, field emission scanning electron microscope (FESEM), high-resolution transmission electron microscopy (HRTEM), X-ray diffraction (XRD), partial size, and surface analysis. Then, it was investigated for the remediation of wastewater from anionic methyl orange (MO) under various adsorption parameters (contact time, adsorbent mass, solution pH, and dye initial concentration). The high adsorption capacity of MO (508.2 mg) had been successfully achieved by Zn–Fe LDH from wastewater within 150 min. It was also known that the pH 7 is optimum value for maximum adsorption, which was the most influencing factor. The adsorption kinetic was governed by pseudo-first (PFO) and -second (PSO) models. The equilibrium adsorption data were obeyed to Langmuir model. Additionally, recyclability was tested up to three cycles of recuperate material after dye adsorption. Lastly, the wasted adsorbent has been tested for the management of another (cationic) dye, methylene blue. The adsorption mechanism was emphasized by FTIR analysis and batch adsorption experiments. The developed LDH could be a strong candidate for traditional adsorbents used in wastewater.

Keywords Zn · Fe LDH · MO · MB · Isothermal · Kinetic models · Recycling

Abbreviations

LDH	Layered double hydroxide
MO	Methyl orange
MB	Methylene blue
FESEM	Field emission scanning electron microscope
HRSEM	High-resolution transmission electron microscopy
EDX	Energy dispersive X-ray
FTIR	Fourier-transform infrared
Ppm	Parts per million
PZC	Point of zero charge
XPS	X-ray photoelectron spectroscopic
XRD	X-ray diffraction
q_{max}	Maximum adsorption capacity (mg g^{-1})
PFO	Pseudo-first order
PSO	Pseudo-second order
q_e	Refers to the amount of adsorbate in the adsorbent at equilibrium (mg g^{-1})
C_0	The initial equilibrium dye concentration (mg L^{-1})
C_e	The equilibrium dye concentration (mg L^{-1})
V	The volume of solution, L
W	The mass of adsorbent used, g
K_L	Langmuir isotherm constant (L/mg)
K_f	Freundlich adsorption capacity (mg g^{-1})
K_{LF}	Langmuir–Freundlich equilibrium constant for heterogeneous solids
$1/n_F$	Freundlich adsorption intensity
n	The empirical constant

✉ Rehab Mahmoud
radwaraft@yahoo.com; DR.Rehab.khaled@science.bsu

1 Environmental Science and Industrial Development Department, Faculty of Postgraduate Studies for Advanced Sciences, Beni-Suef University, Beni-Suef, Egypt

2 Department of Chemistry, Faculty of Science, Beni-Suef University, Beni-Suef 62514, Egypt

مدينة الملك عبدالعزيز
KACST للعلوم والتقنية

⚫ Springer

k1   The pseudo-first-order rate constant, min-1

k2   The rate constant of pseudo-second-order adsorption, g/(mg min)

Introduction

Nanomaterials and nanotechnology are employed to develop novel environment-friendly materials for enabling water remediation (Zhang 2018) and eliminating the environmental pollution greatly induced by conventional ones (Zhang 2016a, 2016b). The designed nanomaterials can detect pollutants in actual time and generating a consistent treatment as needed. Discharging of industrial, municipal, and agricultural wastewaters into environment raise the pollution level in water resources which affect negatively on human and environment (Egirani et al. 2020b, 2017). There are numerous sources of pollution varied from dyes (Ren et al. 2013), heavy metals ions (Egirani et al. 2020a; El-Naggar 2019a, 2019b), pharmaceutical residuals (Shi et al. 2017), organic (Fadali 2014), petrochemicals, pesticides, herbicides (Cicek 2003), and other harmful chemical compounds (Mahgoub 2020; Zaher 2020). However, both of the anionic methyl orange (MO) or cationic methylene blue (MB) are widely used in the various industries processing. These dyes are toxic to human and they consider hazardous to the aquatic system. Therefore, it becomes necessary to eliminate it before discharging again to the ecosystem. Several removal techniques including the biological degradation techniques, normal adsorption methods, and the advanced oxidation processes which were studied to minimize the concentration of such dyes in the water resources.

Layered double hydroxides are considered an anionic clays whose structure is similar to that of brucite (Wan 2016). They have flexibility in structure which allows functional LDHs to be prepared with a wide variety of precursors (Yang 2017). The LDH attracted much attention in the last years owned to their vast applications such as environmental, energy, biotechnology, and nanotechnology (Laipan 2020). LDHs are recorded as strong sorbents for different kinds of pollutants from water like chromate (Matusik and Rybka 2019), phosphate (Hatami et al. 2018), chloride ions (Yoon et al 2014), anionic surfactants (Pavan et al. 2000), dyes (Parida and Mohapatra 2012; Starukh et al. 2016), and humic substances (Li 2020).

In the last years, LDHs took considerable interests for the removal of organic pollutants depending on their unique features and properties including high surface area, low toxicity, high thermal and chemical stabilities, low cost, high anion substitution capacity, and the regeneration ability (El-Reesh 2020). There are several methods of modification for LDHs were reported, for example, ion exchange method, co-precipitation in the presence of organic species,

reconstruction method (Zhang et al. 2020b). Although high adsorption efficiency has been performed, there are important issues need to be taken in consideration. The heart of the applied matter is that larger scale applicability, simple preparation, and lower cost should be matched with the growth preparation of LDH materials. It is presented that LDHs still have some limitations, they cannot be used under high basic or acidic conditions, the possibility of desorption process needs to be considered the possibility of desorption process needs to be considered.

The challenge is applying new methods for the regeneration of LDH materials should be the motivations of future investigations on LDHs, seek advanced modifications, easier to operate, environment friendly in industry, which needs of the majority of scientific researchers.

Zn–Fe LDH was selected as a model due to its low solubility product ($pK_{sp} = 62.51$) and high stability constant ($pK_{formation}$ 25.27) among other LDHs (Boclair and Braterman 1999). On the other hand developing innovative methods to recycle the continuous increment in the quantities of solid adsorbent wastes is critical demand in the contemporary world (Mahgoub 2020). As listed in Table 1, comparison of Zn–Fe LDH with other adsorbents. To further estimate the importance of prepared materials for wastewater remediation from MO, the maximum adsorption capacity (q_{max}) obtained from isotherm models fit of MO on this LDH are carefully compared with those on other adsorbents. By considering the high adsorption capacity, it seems that the as-prepared Zn–Fe LDH can be potentially used for the cost-effective adsorbents for MO-polluted aquatic systems.

In current work, Zn–Fe LDH was synthesized via simple synthesis process and investigated for scavenging of MO at varied different conditions of pH, initial MO concentrations, and equilibrium contact time. The kinetics and isotherms of MO adsorption onto synthesized material were investigated using the batch adsorption method. Also, to support the adsorption research area, the reuse of the formed waste after the adsorption process of MO onto Zn–Fe LDH was performed for MB adsorption purposes.

Materials and methods

Materials

$Fe(NO_3)_3.9H_2O$, methyl orange ($C_{14}H_{14}N_3NaO_3S$), methylene blue ($C_{16}H_{18}ClN_3S.XH_2O$ [X = 2,3]) were supplied from General Drug House, Ltd., India. $Zn(NO_3)_2.6H_2O$ was purchased from Chem-Lab NV, Belgium. Sodium hydroxide [NaOH] was obtained from Piochem for laboratory chemicals, Egypt. The experiments were performed using deionized water which free from CO_2.

Table 1 Maximum adsorption capacities of different LDHs for MO at different process parameters

Adsorbent	Temp (°K)	Initial concn (mg/L)	Equilibrium time (min.)	pH	Adsorption capacity (mg/g)	Ref
Ni–Fe LDH	298	20—200	80	3	246.9	Zubair (2018)
Starch Ni–Fe LDH (2:1) (1:1)			180 120		358.4 387.6	
Ni-LDH Ni-CLDH Mg-LDH Mg-CLDH	298	20—200	240	8	783.65 859.47 576.00 717.73	Elmoubarki (2017)
Ni Al LDH	298	50—500	10–100	3	500.6	Hassani (2017)
Zn–Al–SO$_4$ LDH Zn–Al–Cl LDH Zn–Al–NO$_3$ LDH Zn–Al–CO$_3$ LDH	298	20–1000	300 240 300 240	3.5–4.5	2758 2455 2270 1684	Mahjoubi (2017)
Co–Fe LDH	298	5–300	1440	7	1290	Ling (2016)
Mg$_2$/Fe-CLDH	343	100–1000	30	6–7	194.9	Peng (2015)
Calcined-Mg–Ni–Al LDH	298	20–100	30	8	375.4	Zaghouane-Bou-diaf et al. (2012)
Zn/Al-LDO	298	100	120	6	181.9	Ni (2007)
Zn–Fe LDH	308	20—800	240	7	508.2	This study

Methods

Co-precipitation technique was implemented in this work to synthesis Zn–Fe LDH of nitrate type. Zinc nitrate solution was mixed with iron nitrate to reaches 4:1 of molar ratio. At stable stirring with controlled time adding (slow flow rate 0.10 mL/min), NaOH solution (2 M) was slowly introduced to complete the settling till pH 10. The precipitate was aged at 50 ± 0.5 °C for 12 h, filtered and carefully washed number of times, with bi-distilled water, to obtain material free of excess OH$^-$ and then washing using ethanol. At the end, the achieved precipitate was dried at 60 ± 0.5 °C for 24 h (Moaty et al. 2016).

Characterization

The Zn–Fe LDH was characterized by XRD using PANalytical Empyean, Sweden. The scanning ranged from 10° to 60° with 0.05° step under 30 mA and 40 kV of current and accelerating voltage, respectively. The chemical bonds were detected via their vibration in the range of 400–4000 cm^{-1} using Bruker, vertex 70 FTIR-FT Raman, Germany spectrophotometry (serial number 1341). The morphology of materials was characterized by Gemini (Zeiss-Ultra 55) Field Emission Scanning Electron Microscope. High-resolution transmission electron microscopy images (HRTEM) by JEOL-JEM 2100 (Japan), at 200 kV. The X-ray energy dispersive spectroscopy (EDX) analysis (Quanta FEG250, Germany) was used to confirm the sorbent molar ratio. The surface analyses (area, pores volume, and pores size

distribution) of the sorbent were determined by N$_2$ adsorption using TriStar II 3020, Micrometrics surface analyzer, USA. X-ray photoelectron spectroscopy (Kratos, England) with Al-KαX-ray mono chromatic source, hυ = 1486.6 eV, was used to measure the elemental composition of the prepared material. Zeta potential and hydrodynamic particle size and were investigated as stated in our previous work (Mohamed et al. 2018) using Nano-Zeta sizer supplied from Malvern Instruments Ltd., UK.

Adsorption experiments

Sorption of MO onto Zn–Fe LDH

The batch adsorption runs were happened by shaking vigorously the prepared Zn–Fe LDH with MO solution using orbital shaker (200 rpm) at room temperature. The adsorption parameters were varied like pH (5–11), sorbent dose (0.012–0.30 g), reaction time (0–240 min), and MO initial concentration (20–800 mg L^{-1}). At the end of each run, the solution was filtered using syringe filter, Millipore Millex-G, Hydrophilic PVDF. The concentration of the MO after sorption was detected at wavelength 460 nm using UV-2600, Shimadz spectrophotometer (Japan). To ensure their reproducibility, all runs were triplicated and the average of concentrations values was calculated using SPSS version 16. Means and standard deviation ($\pm$SD) values were calculated, additionally P values < 0.05 were considered to be statistically significant. The efficiency of MO sorption onto Zn–Fe LDH was determined by Eq. 1 (Nijboer and

Verdonschot 2004), the adsorption at equilibrium, q_e (mg/g), was estimated by the Eq. 2 (Delaney 2011):

$$Q\% = \frac{(C_o - C_t)}{C_o} \times 100, \tag{1}$$

$$q_e = \frac{V(C_o - C_e)}{W}, \tag{2}$$

where Q is owned to the adsorptivity (%), C_o expressed in mg/L is referred to the MO initial concentration, and C_t expressed in mg/L is owned to the concentration of MO at time t (min) of adsorption, C_e expressed in mg/L is the MO equilibrium concentration, V (in liter) is owned to solution volume, and W expressed in gram is owned to the sorbent mass.

The isotherms of MO sorption onto Zn–Fe LDH were achieved under three initial concentrations of MO. They were obeyed Langmuir, Freundlich models, and Langmuir–Freundlich. To investigate the process kinetics, 0.035 g of Zn–Fe LDH was introduced at room temperature to 50 mL of MO solution (initial concentrations 5, 10 and 15) for 4 h. Samples were taken at specified time intervals, they were triplicated and average values were register.

The adsorption of MB onto Zn–Fe LDH/MO

The wasted adsorbent (Zn–Fe LDH after MO adsorption) were harvested, centrifuged and washed many times to obtain the Nano composite of Zn–Fe LDH/MO. Finally, the Zn–Fe LDH/MO nanocomposite was dried at 50 ℃ for 24 h then used as new adsorbent for MB management in water. The batch adsorption runs were performed by mixing of 0.025L MB (20 mg/L) with the wasted adsorbent (0.10 g) at room temperature and pH 7.

Results and discussion

Characterization

Morphology study

The morphology of the prepared Zn–Fe LDH was investigated by FESEM photos (Fig. 1). They emphasized characteristic layers, sheets and hexagonal like morphology of LDH. The adsorbent structure consists of hexagonal nanoplateles located on each other, mostly horizontal. This lamellar structure exhibits to some extent disorder status. However, the layers accumulation in this statue may be attributed to the preparation of the adsorbent using

precipitation technique (Pagano 2011), and it is clear that the reaction time and rate play a significant roles on the shape, dimension thickness of these platelets. This may be related to the slow nucleation process (Rahmanian et al. 2018). The high-resolution transmission electron microscope (HRTEM) images of the LDH (Fig. 2) show uniform layers and hexagonals of LDH. The selected area electron diffraction pattern of the sample which was used to further study the crystal structure of Zn–Fe LDH confirms the polycrystalline nature. The Fig. 2e presented the characteristic layered feature of LDH with interplanar spacing around 0.25 nm which match with XRD investigation and the literature for prepared Zn–Fe LDH (Lu 2015). The selected area electron diffraction (SAED) will helped to obtain good insight into the LDH crystalline structure (Fig. 2f). The LDH chemical structure was also emphasized by the X-ray energy dispersive spectroscopy (EDX) analysis. As show in Fig. 3, there are three elements existed in the prepared LDH: iron, zinc, and oxygen.

Surface property

N_2 adsorption/desorption isotherms of the prepared Zn–Fe LDH is shown in Fig. 2g. Referring to the International Union of Pure an Applied Chemistry (IUPAC) classification, the non-attendance of a plateau at the P/P_o near to 1 and the presence of small closed hysteresis loop at relative pressure > 0.8 are owned to isotherms of type II that is characteristic with a hysteresis loop of H3-type resulting from capillary condensation process and mesopores/macroporous construction. There is wide distribution of pore size up to16 nm (Fig. 2h) and the average pore size is < 50 nm. The surface properties of the prepared sample were determined by (BET) Brunauer–Emmett–Teller method. The total pore volume, average pore size, and BET specific area of the sample are 0.078 cm³/g, 2.61 nm and 71.61 m²/g, respectively.

X-ray photoelectron spectroscopy (XPS) was performed to confirm the chemical bonding environment of containing atoms and to analyze the composition. The XPS survey spectrum of Zn- Fe LDH (Fig. 3) confirms the presence of Zn, Fe and O. The high-resolution Zn 2p XPS spectra showed two asymmetric peaks assigned chemical respectively to Zn 2p 1/2 and Zn 2p 3/2 core levels at 1044.7 and 1021.8 eV, which revealed that Zn species were in 2 + oxidation state in LDH structure (Mou 2018; Chen 2011).The O 1 s signals as shown in Fig. 3 of pure LDH was in the binding energy of 531.80 which owned to the hydroxyl group of LDH (Hadnadjev-Kostic 2017; Yi 2018). Also, the Fig. 3showed that the Fe 2p of Fe^{3+} peaks convoluted by Fe 2p3/2 (711.7 eV) and Fe 2p1/2 (725.5 eV) indicate slight positive shift (Zhang et al. 2020a).
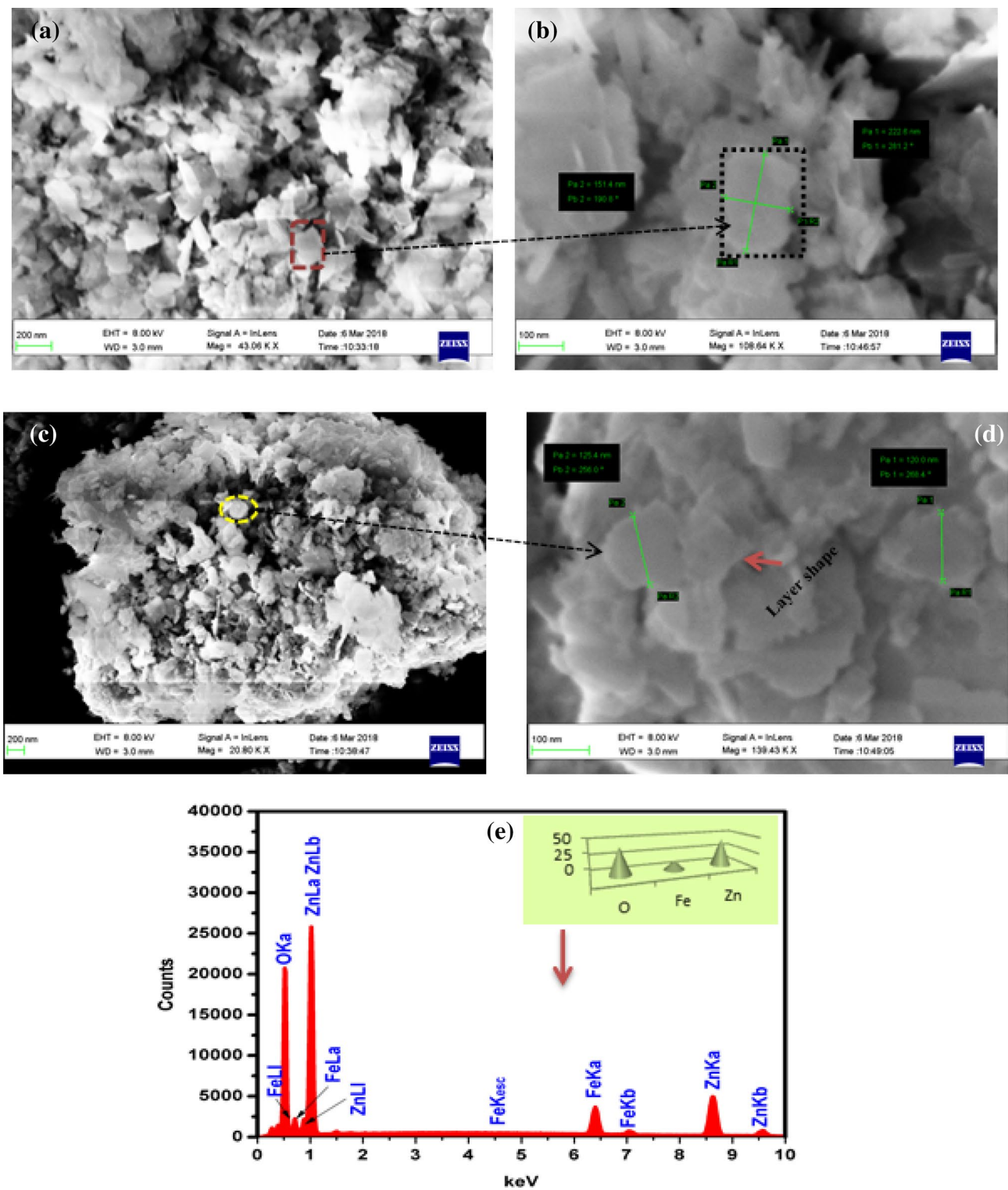
Fig. 1 FESEM images of the **a**–**d** and EDX of the prepared Zn–Fe LDH **e** and the inset figure for the quantitative analysis of the sample elements
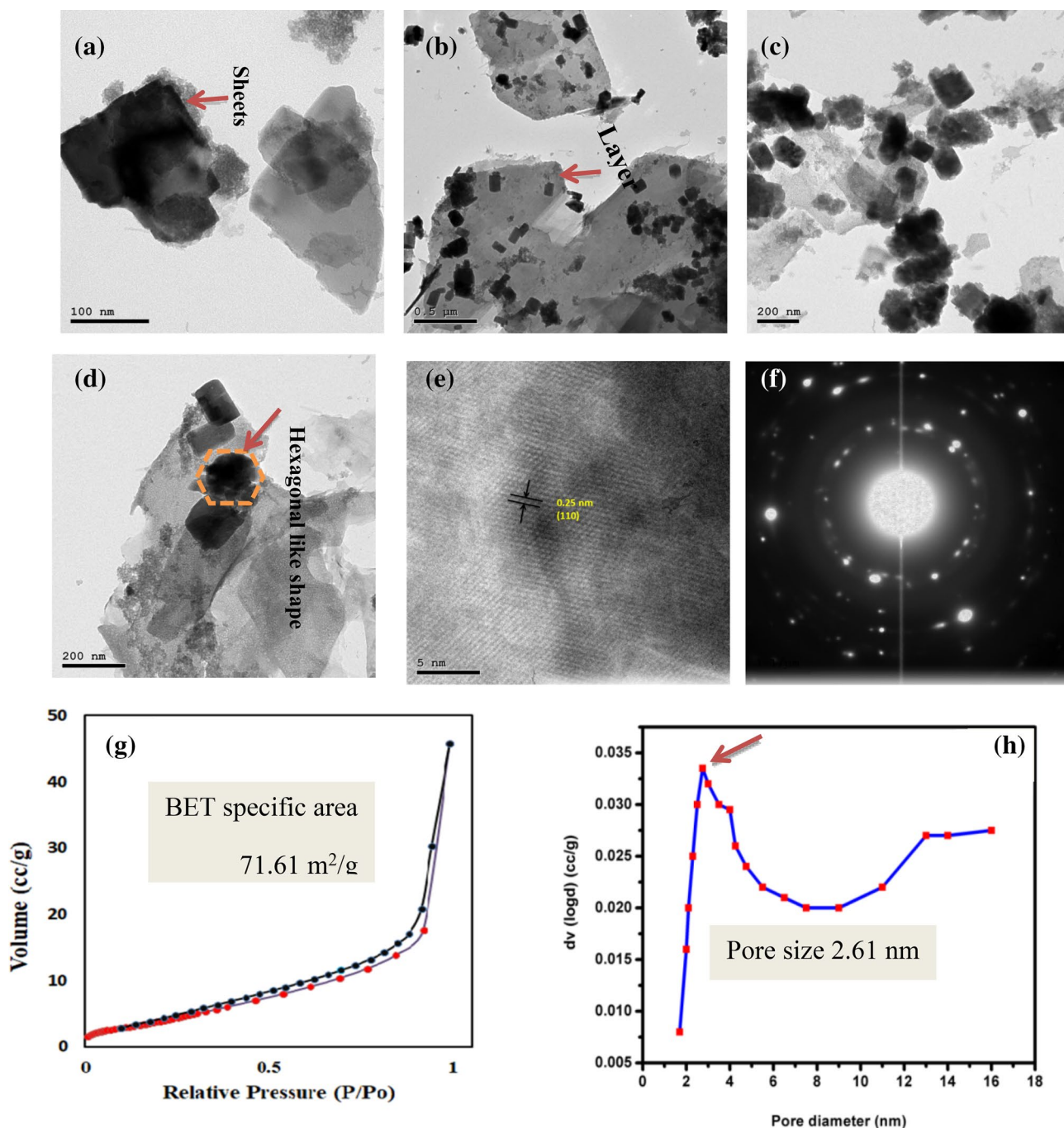
Fig. 2 HRTEM images of the a–d; interplanar spacing (**e**); (SAED) the selected area electron diffraction and N_2 sorption isotherms (**g**) and pore size distribution (**h**) for the prepared Zn–Fe LDH

Fourier transform-infrared of Zn–Fe LDH

The FT-IR spectra of Zn–Fe LDH before/after adsorption of MO and MB are shown in Fig. 4a and Table 2. In the spectrum of Zn–Fe LDH, the infrared bands were around 3772 cm^{-1} which is owned to characteristic free OH stretching of the LDH structure vibration (Mohamed et al. 2018),

with H bonding, and to the water molecules located in the LDH interlayer. Otherwise at 3478 cm^{-1} may attributed to the bonded OH stretching vibration, with H bonding, in addition to the water molecules exist in the LDH interlayer (Younes 2019). At 1635 cm^{-1}, the interlayer water molecules bands show bending vibration. The peak appears at 1378 cm^{-1} was attributed to the ν_3 stretching vibration
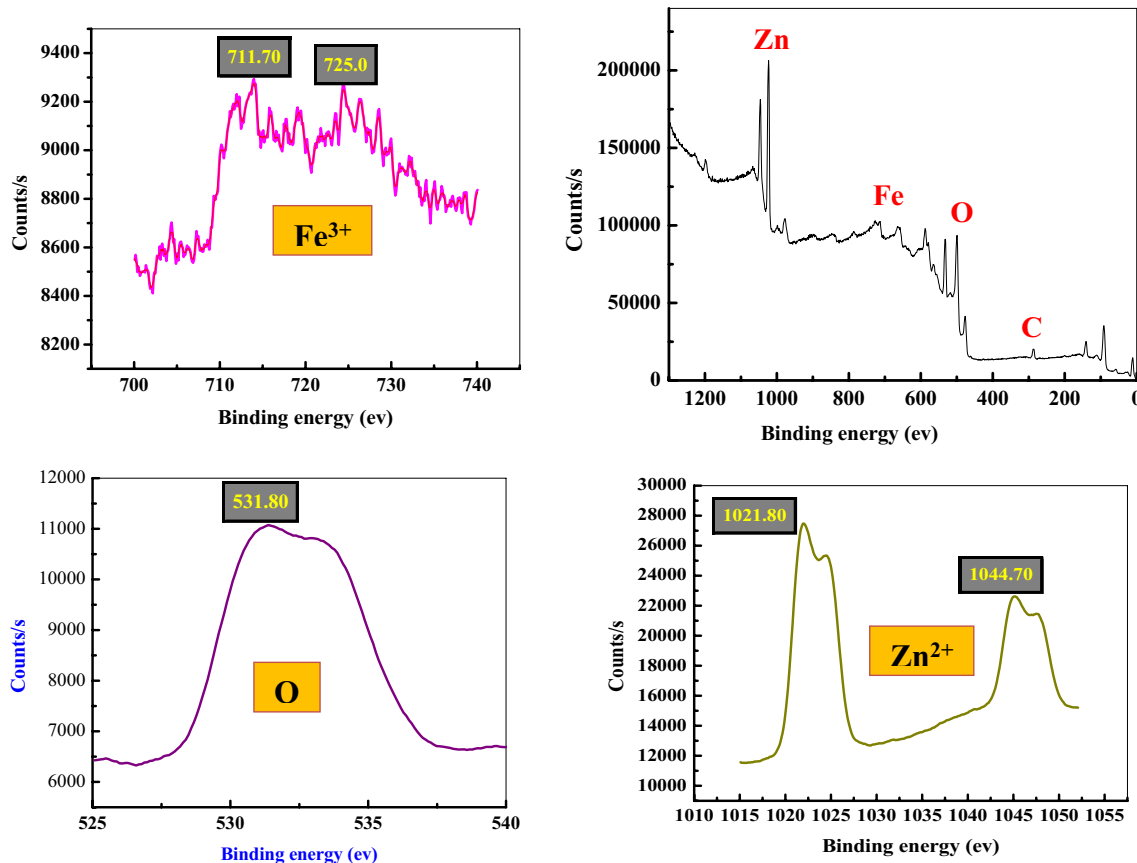
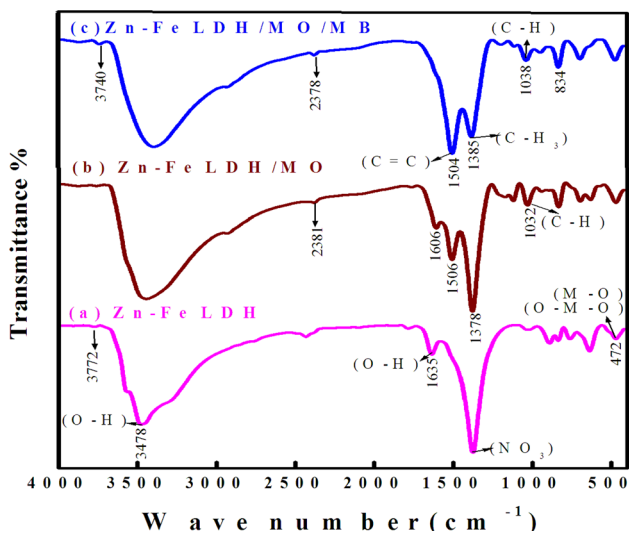**Fig. 3** XPS spectra of Zn–Fe LDH, Zn 2p, O 1 s and Fe 2p

Fig. 4 A comparison of FT-IR spectra of Zn–Fe LDH (**a**), after MO adsorption (Zn–Fe LDH/MO) (**b**) after MB adsorption (Zn–Fe LDH/MO/MB) (**c**)

of the interlayer NO_3 groups. The bands under 1000 cm^{-1} resulted from M–O–M, O–M–O and M–O vibrations in the

brucite-like layers (Moaty et al. 2016; Younes 2019; Nejati 2018).

X-ray diffraction analysis

The XRD patterns of Zn–Fe NO_3 LDH showed characteristic reflections corresponding to a crystalline layered phase (Nejati 2018) (Fig. 5). In the range of $2\theta = 6–80°$, the strong and sharp diffraction peaks at low 2θ values. The basal spacing value of the LDH phase, representing the summation of the thickness of the brucite-like layer (0.414 nm) which is good agreement with that of the nitrate LDH materials with reference code (04-018-3495). The layered structure of the Zn–Fe LDH is confirmed by the presence of the main peaks at 2θ at 9.14°, 25.34°, 31.86 °, 39.01°, 47.70° and 56.90° (Lu 2018). The formation of free hydroxide was not appeared in the XRD chart which may be related to slow addition of sodium hydroxide during the LDH formation. We notice that the peaks are narrow, reflecting that the substitution of Fe and Zn into the crystalline Zn–Fe LDH structure were performed (Zhu 2014; Naseem 2019). Since the intensity of peaks for (003) is higher than that for (015) and (009), the formation of partly delaminated LDH is probable (Gupta

Table 2 A conclusion for the bands and assignments for Zn–Fe LDH before and after MO& MB adsorption

Wave number (cm^{-1})			Assignment	
Zn–Fe LDH	Zn–Fe LDH/MO	Zn–Fe LDH/MO/MB		
3772 (w)	–	3740 (w)	3772	Free OH-stretching vibration (Moaty et al. 2016)
			3740	
3478 (b.)	3442 (b.)	3395 (b)	3478	Bonded OH-stretching vibration (Younes 2019)
			3442	N–H stretching vibration (Shen 2015)
			3395	Stretching vibration of a hydrogen bond with OH group (Ovchinnikov 2007)
–	2381 (w)	2378 (w)	2381	C–N overtone
		2315 (w)	2378	(H$_3$C) -N- (CH$_3$) (Ovchinnikov 2007)
			2315	
1635 (m)	1606 (w)	–	1635	Bending vibration of the interlayer water molecules (Nejati 2018)
			1606	C–C vibration of the benzene structure (Shen 2015)
–	1506 (m)	1504 (s)	1506	C–C vibration of the benzene structure (Shen 2015)
			1504	
1378 (s)	1378 (s)	1385 (m)	1378	ν_3 stretching vibration of the NO$_3$ (Nejati 2018)
			1378	Stretching vibration of C-N
			1385	1. C–N stretching vibration 2. Bonded C–H$_3$ vibration (Ovchinnikov 2007)
–	1178 (w)	1198 (w)	1178	Stretching vibration C–C and/or C–N
		1115 (w)	1198, 1115	The vibrations of heterocycle structure (Ovchinnikov 2007)
–	1121 (m)		1121	S = O vibration (Shen 2015)
–	1032 (m)	1038 (m)	1032,1038	The benzene ring had C–H stretching vibration (Ovchinnikov 2007)
891 (m)	941 (w)	949 (w)	all	The M–O–H lattice vibrations (Nejati 2018)
837 (w)	834 (m)	834 (m)	837	deformation modes (weak out of-plane symmetric ν_2 and the anti-symmetric ν_4) of nitrate (Mahjoubi 2017)
			834	The benzene ring had C–H stretching vibration (Ovchinnikov 2007)
639 (m)	632 (w)	696 (m)		C–S stretching vibrations (Shen 2015)
472 (m)	472 (m)	474 (m)		Bands resulted from M–O–M, M–O and O–M–O vibrations in brucite-like layers (Younes 2019)
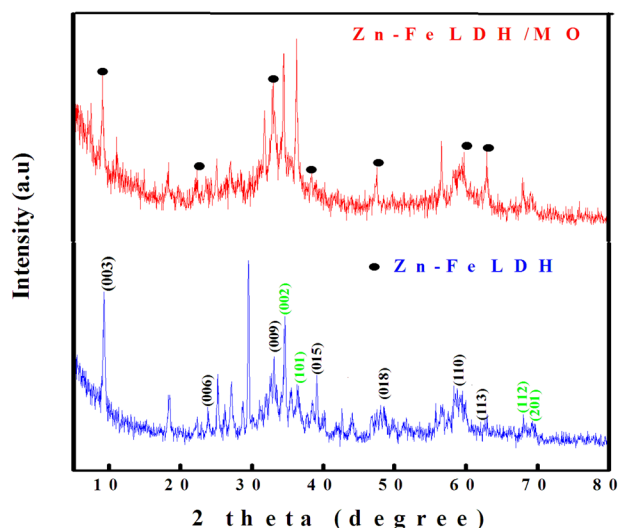
Fig. 5 XRD pattern of Zn–Fe LDH before and after MO adsorption

2020) and this matches with the new morphology in the SEM for LDH. Also, the diffraction peaks located at 31.60◦, 34.69◦, 36.48◦, 62.84◦, 67.90◦, and 69.44◦ have been indexed as hexagonal phase of ZnO (Talam et al. 2012).

Adsorption of MO onto Zn–Fe LDH

Effect of the solution pH on the adsorption process

A variation in pH results in alteration in the chemistry of adsorbent surface and also the ionization degree (Tchuifon 2014) resulting in a significant impact on the adsorption process. Batch adsorption experiments were conducted by varying the solution pH from 3 to 11. MO gains a negative charge beyond pH 4 because its dissociation constant 3.47 (Fig. 6a). The adsorption reached its maximum value at pH 7, beyond this value, the adsorption decreased (Fig. 6a). It was hard to maintain the equilibrium in alkaline medium
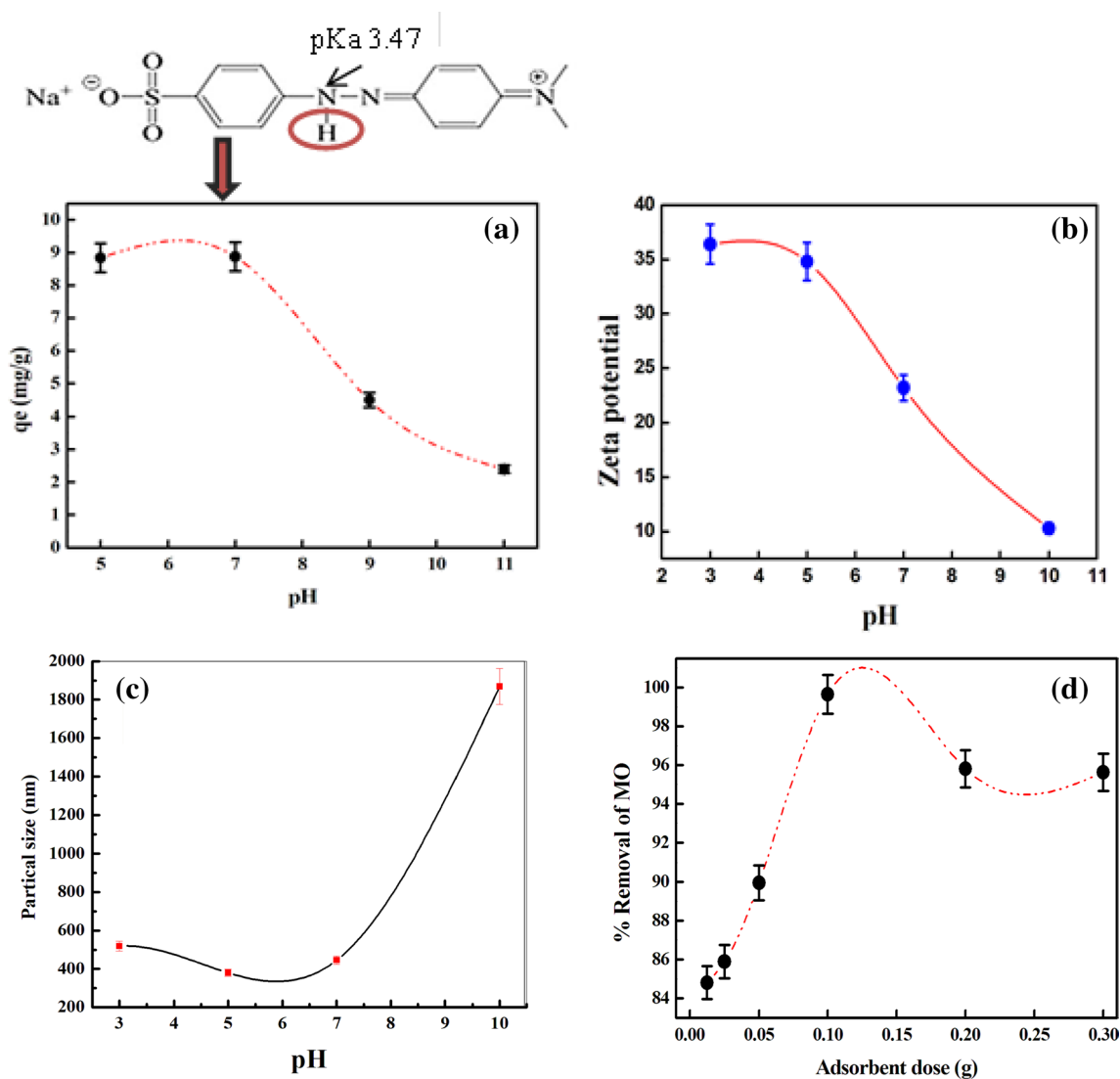
Fig. 6 MO adsorption equilibrium (**a**); zeta potential (**b**); partical size distribution of Zn–Fe LDH at various pH values (**c**) and dose of Zn–Fe LDH on the removal present of MO(d)

due to the high values of OH⁻ that compete with anionic MO which hinder the adsorption equilibrium (Fig. 6a). At acidic solution, MO is protonated due to the possibility of protons to combine with its nitrogen–nitrogen double bond by one nitrogen, adsorption percent decreased as resulted from electrostatic repulsion forces (Arshadi 2014).

Zeta potential is a technique to study the nanoparticles stability and dispersion in solution (Fig. 6b).The zeta potential of the particles is defined as the electric potential or the charge at the boundary of the double layer on the material surface. Also, dispersion, flocculation or aggregation can be measured from the data. The high stability of the Zn–Fe LDH nanoparticles dispersions are related to their high positive zeta potential in large pH range (2–10), leading to strong particle–particle

repulsions. Also, to realize the surface property and surface charge for adsorption behavior of Zn–Fe LDH toward MO dye, the positive zeta potential of adsorbent confirmed the electrostatic interaction between Zn–Fe LDH and MO and favors the adsorption process. At increased pH, the positivity of the adsorbent decrease which decrease the attraction of the negatively charged MO species (Fig. 6c). So, we investigate the practical size distribution (DLS) measurements to confirm the stability of the partial in different medium (Fig S1). As shown in Fig. 6c, the smaller hydrodynamic sized Zn–Fe LDH higher zeta potential and better aquatic stability than larger ones (Fig. S2). Also, they would have long-time used as potential adsorbent for various pollutants in the aquatic systems. (Table S1).

Effect of dose of Zn–Fe LDH on the adsorption of MO

Figure 6d presents the results for MO removal efficiency with different Zn–Fe LDH dose (0.0125–0.30 g) was used per 25 mL MO solution at pH 7. Increasing of MO with increasing adsorbent dose up to 0.10 g and this may be as a result of increasing available active sites for adsorption. Furthermore, the uptake efficiency of the MO decrease with increasing the Zn–Fe LDH dose, this could be due to the aggregation of used LDH particles were happened. Under the optimized pH conditions, at pH 7, the charge of the partials were positive (Fig. 6b), with increase the dose of adsorbent, the strong hydrophobicity, and so enhanced van der Waals interaction drove force of the LDH to aggregate (Ren 2018; Wu 2013). The origin of van der Waals attraction is induced dipoles, a bulk material with electronic or molecular structure that favors generation of permanent or induced dipoles that promote aggregation. Also, interaction of the adsorbent surfaces with water molecules involves a significant entropic penalty driving an aggregation process that may be occurred (Hotze et al. 2010).

So, using small amount of adsorbent is preferable, resulting in decreasing the overall process cost. Additionally, using small amounts of nanoparticles is familiar in industry, and increasing the weight will result negative impact. We can conclude that there is an optimum amount of adsorbent to remove MO, i.e., 0.10 mg of the Zn–Fe LDH adsorbent could manage 20 ppm of MO, and above this value the process is useless. Finally, increasing the adsorbent amount in the large scale will cause additional problem in the environment as it will increase the amount of sludge after treatment.

Adsorption isotherms

MO adsorption onto Zn–Fe LDH

Adsorption isotherms are important to explain the adsorption nature and mechanism. In economical view, isotherm testing can be used for design and optimization of economical adsorption systems. The Zn–Fe LDH proved that it is one of the best adsorbents for the MO adsorption from water. Figure 7 displays the experimental data
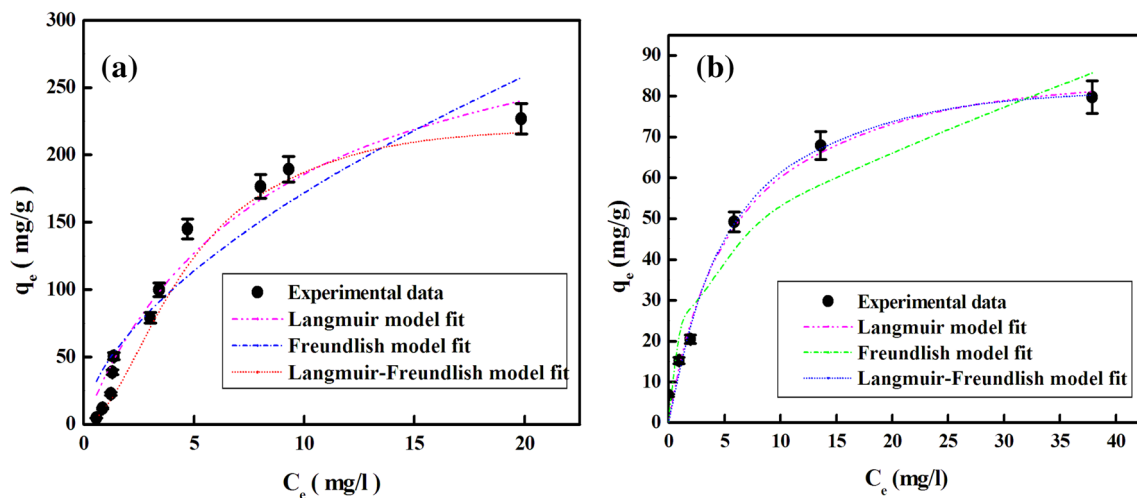

Fig. 7 Experimental data for MO adsorption on Zn–Fe LDH (**a**) and MB adsorption on Zn–Fe LDH/MO (**b**) fitted by the non linear isotherm models. The error bar for standard deviation reflect the triplicate experiments

Table 3 The adsorption isotherm and kinetics models *

Isotherm models	Equations [14, 48]	Kinetics models	Equations [14]
Langmuir	$q_e = \frac{q_{max} K_L C_e}{1 + K_L C_e}$	Pseudo-first order	$q_t = q_e \left(1 - e^{-k_1 t}\right)$
Freundlich	$q_e = K_f C_e^{1/n_F}$	Pseudo-second order	$q_t = \frac{q_e^2 k_2 t}{1 + q_e k_t t}$
Langmuir–Freundlich	$q_e = \frac{q_{max} \left(K_{LF} C_e\right)^{\beta_{LF}}}{1 + \left(K_{LF} C_e\right)^{\beta_{LF}}}$		
		Intraparticle diffusion	$q_t = k_{ip} \sqrt{t} + c_{ip}$

*The adjustable isotherm/kinetics model parameters are defined in the list of symbols

Table 4 The isotherm parameters for the sorption of MO onto Zn–Fe LDH and MB sorption onto Zn–Fe LDH/MO

Adsorption models	The parameters for the sorption of MO onto Zn–Fe LDH	The parameters for the sorption of MB onto Zn–Fe LDH/MO
Langmuir	$q_{max} = 508.2$ mg/g	$q_{max} = 92.95$ mg/g
	$K_L = 0.0673$ L/mg	$K_L = 0.181$ L/mg
	$R^2 = 0.96$	$R^2 = 0.98$
Freundlich	$K_f = 33.08$ mg/g	$K_f = 21.78$ mg/g
	$1/n_F = 0.8103$	$1/n_F = 0.377$
	$R^2 = 0.95$	$R^2 = 0.93$
Langmuir–Freundlich	$q_{max} = 230.72$ mg/g	$q_{max} = 88.33$ mg/g
	$K_{LF} = 0.217$ L/mg	$K_{LF} = 0.205$ L/mg
	$\beta_{LF} = 1.86$	$\beta_{LF} = 1.12$
	$R^2 = 0.99$	$R^2 = 0.99$

from the non-linear adsorption isotherm model Equations (Table 3). As observed in Fig. 7 and Table 4, as well as the high regression coefficient, the adsorption of MO on Zn–Fe LDH could well fitted by three models. The calculating adsorption capacity (q_{max}) of MO was up to 508.20 mg/g. These experimental results demonstrate that this Zn–Fe LDH is an excellent adsorbent Table 4.

The effect of MO adsorption on the Zn–Fe LDH was estimated using the FT-IR analysis of the adsorbent after the up take process (Fig. 4b). The deformation modes (anti-symmetric, ν_4 and plane symmetric, ν_2) of NO_3 observed in LDH spectrum around 903 cm^{-1} while observed at 837 cm^{-1} in Zn–Fe LDH/MO spectrum (Mahjoubi 2017). The characteristic of Zn–Fe LDH peaks were shifted after the MO adsorption towards higher frequencies suggesting new bond has been formed and, the peaks were observed at 3442 cm^{-1} for the N–H stretching vibration, and the peak at 2381 cm^{-1} were indicated C–N overtone. The peaks were located at 1606 cm^{-1} referred to C–C vibration of the benzene structure of MO. The peak located at 1178 cm^{-1} and 1378 cm^{-1} were assigned to stretching vibration of C–C and C–N respectively. The benzene ring had C–H stretching vibration peaks were located at 1032 cm^{-1}, 837 cm^{-1}, the peaks present at 632 cm^{-1} indicated the C–S stretching vibrations (Table 2). Also, by comparison of XRD patterns before and after the MO sorption, the peaks at 31.84° to 31.69°, 36.35° to 36.21° were decreased and that located at 56.67° to 59.92° were increased, while the remained peaks stay unchanged (Fig. 5b). The crystallite size for Zn–Fe LDH and Zn–Fe LDH/MO was calculated to be 49.7 nm and 65.4 nm, respectively. Also, we find that d spacing value was 3.025 and 2.475 Å for LDH and LDH/MO. The decreasing of the d spacing value related to the adsorption of MO at the surface of LDH, this confirm the adsorption of MO process on using prepared adsorbent (Mohammed 2020).

MB adsorption onto Zn–Fe LDH/MO nanocomposite

The Zn–Fe LDH/MO proved that it is one of the best adsorbents for the MB adsorption from water. Figure 7b displays the experimental data from the non-linear adsorption isotherm model Equations (Table 3). As observed in Fig. 7b and Table 4, as well as the high regression coefficient, the adsorption of MB on Zn–Fe LDH/MO could well fitted by three models. The calculating adsorption capacity (q_{max}) of MB was up to 90 mg/g. These experimental results demonstrate that this Zn–Fe LDH/MO is an excellent adsorbent (Table 3). From FT-IR analysis before and after adsorption (Fig. 4c) one can conclude the nature of adsorption of MB onto Zn–Fe LDH/MO nanocomposite (Table 4).

Kinetic studies

Adsorption kinetics models of MO adsorption onto Zn–Fe LDH

The importance of equilibrium time rise from its effect on the applicability and the cost of the adsorption process. The adsorption of MO onto Zn–Fe LDH at different initial concentrations was investigated to determine the equilibrium time of the adsorption process. Then, the data were fitted to three kinetic models. Figure 8 shows the impact of the contact time on the adsorption of MO solution (pH 7) of concentrations of 5, 10, 15 mg/L onto Zn–Fe LDH (0.1 g) at 35 ± 0.5 °C. The MO adsorption occurred in fast rate during the first 25 min of the process, and then the rate of adsorption decreased until the equilibrium is achieved within 150 min.

Based on the correlation coefficient R^2, it has been proven that both the pseudo-second order and the pseudo-first order were the best fit kinetic models with the smallest R^2 close
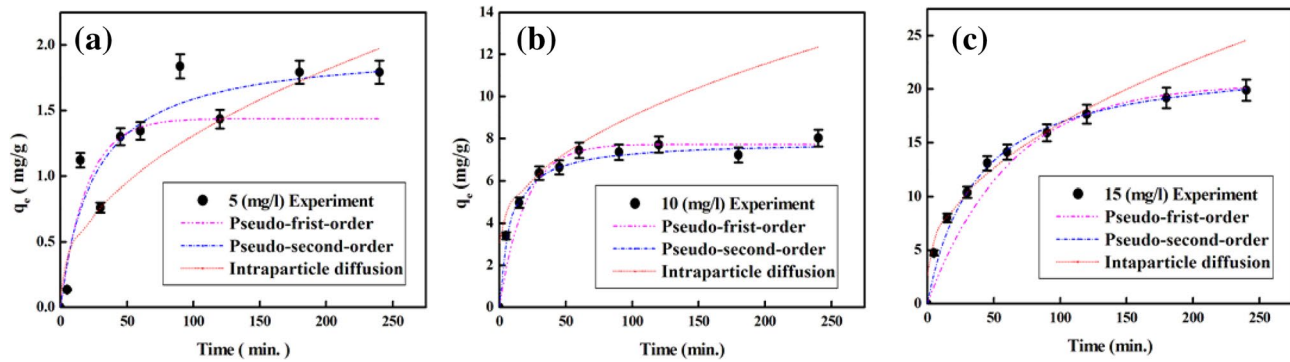
Fig. 8 The adsorption kinetics models with experimental data of MO adsorption onto Zn–Fe LDH at concentrations 5 mg/L (**a**) 10 mg/L (**b**) 15 mg/L (**c**)

Table 5 The parameters of kinetic models for the MO adsorption onto Zn–Fe LDH and adsorption of MB adsorption onto Zn–Fe LDH/MO

Dye	Pseudo-first order				
	C_o (mg/L)	$q_{e,exp}$ (mg/g)	k_1 (min^{-1})	$q_{e,cal}$ (mg/g)	R^2
	5	1.15	0.05	1.44	0.82
MO	10	5.91	0.05	7.72	0.93
	15	12.30	0.016	20.5	0.94
MB	20	4.92	0.93	5.6	0.99
Dye	Pseudo-second order				
	C_o (mg/L)	$q_{e,exp}$(mg/g)	k_2(g/mg.min)	$q_{e,cal}$	R^2
	5	1.15	0.02	1.99	0.89
MO	10	5.91	0.015	7.87	0.98
	15	12.30	0.001	23	0.98
MB	20	4.92	1.53	5.8	0.99
Dye	Intraparticle diffusion				
	C_o (mg/L)	$q_{e,exp}$(mg/g)	K_{ip}(mg/g min$^{(1/2)}$)	C_{ip} (mg/g)	R^2
	5	1.15	0.121	0.098	0.78
MO	10	5.91	0.598	3.085	0.75
	15	12.30	1.43	1.07	0.83
MB	20	4.92	0.291	1.69	0.62

to unity ($R^2 = 0.98$ and 0.94 for both models respectivelly) (Table 5).

Adsorption kinetics models of MB adsorption onto Zn–Fe LDH/MO

The impact of time on MB sorption onto the recycled adsorbent was also studied (Fig. 9), the equilibrium time was very fast (5 min) compared to the MO adsorption onto the same adsorbent. This refers to that the adsorption of the cationic MB occurred onto the external surface area via the new functional groups that developed by introducing of MO to Zn–Fe LDH surface.

The three kinetic models were investigated for the MB adsorption onto Zn–Fe LDH/MO, both models (PFO and PSO) describe well the practical data (R^2 0.99). And also the calculated data are close to the experimental one. The intraparticle diffusion did not govern the kinetic of MB adsorption process onto Zn–Fe LDH/MO where the calculated data did not match with the experimental one. This refers to that MB adsorption onto Zn–Fe LDH/MO occurs through chemical and physical interaction (Table 5).

Reusability of the Zn–Fe LDH for MO adsorption

The management of the wasted adsorbent was done via two scenarios the adsorbent was reused for the adsorption of the
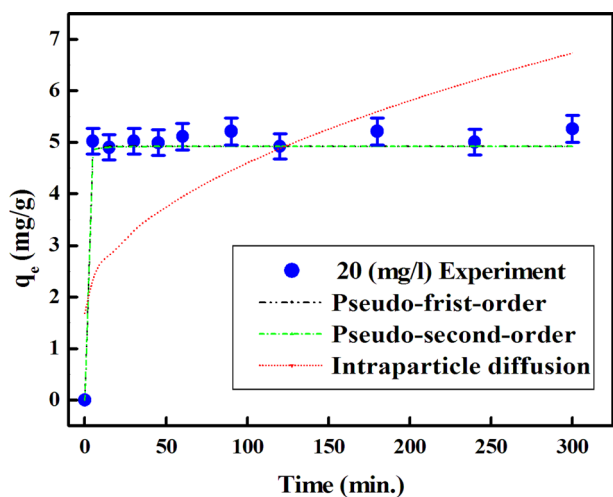
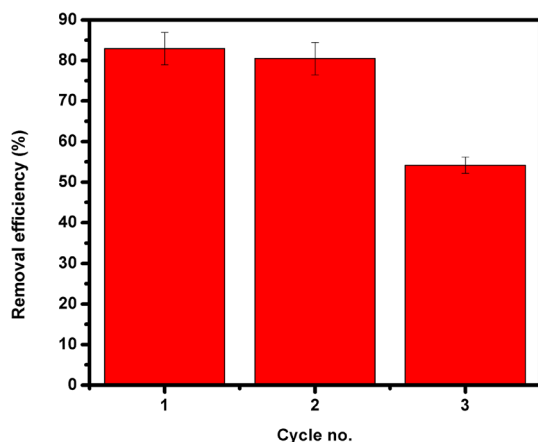**Fig. 9** Comparison of adsorption kinetics models with experimental data of MB dye on Zn–Fe LDH/MO

Fig. 10 Multi-cyclic adsorption of MO onto Zn–Fe LDH ($V = 0.025$ L, Co $= 20$ ppm, $T = 35 \pm 0.5$ °C, pH $= 7$)

(MO). The results of Zn–Fe LDH recycling are illustrated in Fig. 10. It is of important to investigate the availability of reusability performance of the Zn–Fe LDH to evaluate their economic condition. As presented at Fig. 10, and this means that these materials have a good regeneration behavior. The removal efficiencies of three recycles was 83, 80 and 54% have been achieved. This added value gains the adsorbent new merits like decreasing the amount of wasted adsorbent, reducing the adsorbent cost and finally produces multifunctional adsorbent.

Conclusion

In the current research, Zn–Fe LDH was prepared using a simple co-precipitation way and applied as an efficient adsorbent for the removal of anionic dye MO from aqueous solution. Up on batch uptake experiments, it was found that the adsorption efficiency was greatly affected by pH, adsorbent dose, concentration and time, showing a high adsorption capacity at pH 7, for an adsorbent dose of 0.10 g at a temperature of 35 °C. Also, the adsorption process of MO on Zn–Fe LDH was characterized and ascertain using different techniques such as FTIR spectroscopy, XRD, FESEM, HRTEM, zeta potential, partial size and surface area analysis. The equilibrium adsorption data were investigated using three isothermal models, where the q_{max} was determined to be 508.20 mg/g. Also, the waste Zn–Fe LDH/MO was reused as new adsorbent for cationic dye MB. The adsorption process is controlled kinetically for MO or MB adsorption by the second-order reaction through physical adsorption. The characterization was performed before and after adsorption. The adsorption mechanism on Zn–Fe LDH was investigated using FTIR and XRD analysis.

Compliance with ethical standards

References

Arshadi M et al (2014) Adsorption studies of methyl orange on an immobilized Mn-nanoparticle: kinetic and thermodynamic. RSC Adv 4(31):16005–16017

Boclair JW, Braterman PS (1999) Layered double hydroxide stability. 1. Relative stabilities of layered double hydroxides and their simple counterparts. Chem Mater 11(2):298–302

Chen C et al (2011) Enhanced Raman scattering and photocatalytic activity of Ag/ZnO heterojunction nanocrystals. Dalton Trans 40(37):9566–9570

Cicek N (2003) A review of membrane bioreactors and their potential application in the treatment of agricultural wastewater. Can Biosyst Eng 45:6.37

Delaney P et al (2011) Development of chemically engineered porous metal oxides for phosphate removal. J Hazard Mater 185(1):382–391

Egirani DE et al (2020a) Optimization of cobalt content management in wastewater using wasif and bayda clay composites. J Chem Technol Metall 55(4):801

Egirani D, Poyi N, Shehata N (2020b) Preparation and characterization of powdered and granular activated carbon from Palmae biomass for cadmium removal. Int J Environ Sci Technol 27:1–12

El Hassani K et al (2017) Effect of morphological properties of layered double hydroxides on adsorption of azo dye methyl orange: a comparative study. Appl Clay Sci 140:124–131

Elmoubarki R et al (2017) Ni/Fe and Mg/Fe layered double hydroxides and their calcined derivatives: preparation, characterization and application on textile dyes removal. J Mater Res Technol 6(3):271–283

El-Naggar DEEM et al (2019a) Ion exchangers as an emerging technique for removal of toxic heavy metals in wastewater: a review. Appl Radiat Isot 146:18–23

El-Naggar I et al (2019b) A novel approach for the removal of lead (II) ion from wastewater using Kaolinite/Smectite natural composite adsorbent. Appl Water Sci 9(1):7

EL-Rabiei M et al (2017) Evaluation of carbon nanotubes (CNTs) in management of a full scale centralized wastewatertreatment plant. Res J Pharm Biol Chem Sci 8(4):1180–1190

El-Reesh GYA et al (2020) Novel synthesis of Ni/Fe layered double hydroxides using urea and glycerol and their enhanced adsorption behavior for Cr (VI) removal. Sci Rep 10(1):1–20

Fadali OA et al (2014) Effect of lag-phase in the transition from oxic to anoxic conditions on the performance of the sequencing batch reactor. Int J Innov Appl Stud 7(1):393

Gupta NK et al (2020) Microscopic, spectroscopic, and experimental approach towards understanding the phosphate adsorption onto Zn–Fe layered double hydroxide. J Mol Liq 297:111935

Hadnadjev-Kostic M et al (2017) Photo-induced properties of photocatalysts: a study on the modified structural, optical and textural properties of TiO2–ZnAl layered double hydroxide based materials. J Clean Prod 164:1–18

Hatami H, Fotovat A, Halajnia A (2018) Comparison of adsorption and desorption of phosphate on synthesized Zn-Al LDH by two methods in a simulated soil solution. Appl Clay Sci 152:333–341

Hotze EM, Phenrat T, Lowry GV (2010) Nanoparticle aggregation: challenges to understanding transport and reactivity in the environment. J Environ Qual 39(6):1909–1924

Laipan M et al (2020) Functionalized layered double hydroxides for innovative applications. Mater Horiz 7(3):715–745

Li S et al (2020) Adsorption of humic acid from aqueous solution by magnetic Zn/Al calcined layered double hydroxides. Appl Clay Sci 188:105414

Ling F et al (2016) A novel CoFe layered double hydroxides adsorbent: high adsorption amount for methyl orange dye and fast removal of Cr (VI). Microporous Mesoporous Mater 234:230–238

Lu H et al (2015) Simultaneous removal of arsenate and antimonate in simulated and practical water samples by adsorption onto Zn/Fe layered double hydroxide. Chem Eng J 276:365–375

Lu H et al (2018) Enhanced adsorption performance of aspartic acid intercalated Mg-Zn-Fe-LDH materials for arsenite. Dalton Trans 47(14):4994–5004

Mahgoub SM et al (2020) Sustainable waste management and recycling of Zn–Al layered double hydroxide after adsorption of levofloxacin as a safe anti-inflammatory nanomaterial. RSC Adv 10(46):27633–27651

Mahjoubi FZ et al (2017) Zn–Al layered double hydroxides intercalated with carbonate, nitrate, chloride and sulphate ions: Synthesis, characterisation and dye removal properties. J Taibah Univ Sci 11(1):90–100

Matusik J, Rybka K (2019) Removal of chromates and sulphates by Mg/Fe LDH and heterostructured LDH/halloysite materials: Efficiency, selectivity, and stability of adsorbents in single-and multi-element systems. Materials 12(9):1373

Moaty SA, Farghali A, Khaled R (2016) Preparation, characterization and antimicrobial applications of Zn-Fe LDH against MRSA. Mater Sci Eng C 68:184–193

Mohamed F, Abukhadra MR, Shaban M (2018) Removal of safranin dye from water using polypyrrole nanofiber/Zn-Fe layered double hydroxide nanocomposite (Ppy NF/Zn-Fe LDH) of enhanced adsorption and photocatalytic properties. Sci Total Environ 640:352–363

Mohammed AN et al (2020) Exploitation of new approach to control of environmental pathogenic bacteria causing bovine clinical mastitis using novel anti-biofilm nanocomposite. Environ Sci Pollut Res 27:1–15

Mou H et al (2018) Design and synthesis of porous Ag/ZnO nanosheets assemblies as super photocatalysts for enhanced visible-light degradation of 4-nitrophenol and hydrogen evolution. Appl Catal B 221:565–573

Naseem S et al (2019) Comparison of transition metal (Fe Co, Ni, Cu, and Zn) containing tri-metal layered double hydroxides (LDHs) prepared by urea hydrolysis. RSC Adv 9(6):3030–3040

Nejati K et al (2018) Zn–Fe-layered double hydroxide intercalated with vanadate and molybdate anions for electrocatalytic water oxidation. New J Chem 42(4):2889–2895

Ni Z-M et al (2007) Treatment of methyl orange by calcined layered double hydroxides in aqueous solution: adsorption property and kinetic studies. J Colloid Interface Sci 316(2):284–291

Nijboer RC, Verdonschot PF (2004) Variable selection for modelling effects of eutrophication on stream and river ecosystems. Ecol Model 177(1–2):17–39

Ovchinnikov O et al (2007) Analysis of interaction between the organic dye methylene blue and the surface of AgCl (I) microcrystals. J Appl Spectrosc 74(6):809–816

Pagano M et al (2011) Degradation of chlorobenzene by Fenton-like processes using zero-valent iron in the presence of Fe3+ and Cu2+. Environ Technol 32(2):155–165

Parida K, Mohapatra L (2012) Carbonate intercalated Zn/Fe layered double hydroxide: a novel photocatalyst for the enhanced photo degradation of azo dyes. Chem Eng J 179:131–139

Pavan PC, Crepaldi EL, Valim JB (2000) Sorption of anionic surfactants on layered double hydroxides. J Colloid Interface Sci 229(2):346–352

Peng C et al (2015) Calcined Mg-Fe layered double hydroxide as an absorber for the removal of methyl orange. AIP Adv 5(5):057138

Rahmanian O, Amini S, Dinari M (2018) Preparation of zinc/iron layered double hydroxide intercalated by citrate anion for capturing Lead (II) from aqueous solution. J Mol Liq 256:9–15

Ren N, Zhou X, Guo W, Yang S (2013) A review on treatment methods of dye wastewater. CIESS J 64:84–94

Ren X et al (2018) Graphene analogues in aquatic environments and porous media: dispersion, aggregation, deposition and transformation. Environ Sci Nano 5(6):1298–1340

Shen T et al (2015) A TiO 2 modified abiotic–biotic process for the degradation of the azo dye methyl orange. RSC Adv 5(72):58704–58712

Shi X, Leong KY, Ng HY (2017) Anaerobic treatment of pharmaceutical wastewater: a critical review. Biores Technol 245:1238–1244

Starukh G, Rozovik O, Oranska O (2016) Organo/Zn-Al LDH nanocomposites for cationic dye removal from aqueous media. Nanoscale Res Lett 11(1):228

Talam S, Karumuri SR, Gunnam N (2012) Synthesis, characterization, and spectroscopic properties of ZnO nanoparticles. ISRN Nanotechnol 2012:1

Tchuifon D et al (2014) Equilibrium and kinetic modelling of methyl orange adsorption from aqueous solution using rice husk and egussi peeling. Int J Chem Sci 12(3):741–761

Wan J et al (2016) Tuning two-dimensional nanomaterials by intercalation: materials, properties and applications. Chem Soc Rev 45(24):6742–6765

Wu L et al (2013) Aggregation kinetics of graphene oxides in aqueous solutions: experiments, mechanisms, and modeling. Langmuir 29(49):15174–15181

Yang D et al (2017) Rational design and synthesis of monodispersed hierarchical SiO2@ layered double hydroxide nanocomposites for efficient removal of pollutants from aqueous solution. Chem Eng J 323:143–152

Yi J et al (2018) One step pyridine-assisted synthesis of visible-light-driven photocatalyst Ag/AgVO3. Adv Powder Technol 29(2):319–324

Yoon S, Moon J, Bae S, Duan X, Giannelis EP, Monteiro PM (2014) Chloride Adsorption by Calcined Layered Double Hydroxides in Hardened Portland Cement Paste[J]. Mater Chem Phy 3(145):376–386. https://doi.org/10.1016/j.matchemphys.2014.02.02

Younes HA et al (2019) Computational and experimental studies on the efficient removal of diclofenac from water using ZnFe-layered double hydroxide as an environmentally benign absorbent. J Taiwan Inst Chem Eng 102:297–311

Zaghouane-Boudiaf H, Boutahala M, Arab L (2012) Removal of methyl orange from aqueous solution by uncalcined and calcined MgNiAl layered double hydroxides (LDHs). Chem Eng J 187:142–149

Zaher A et al (2020) Zn/Fe LDH as a clay-like adsorbent for the removal of oxytetracycline from water: combining experimental results and molecular simulations to understand the removal mechanism. Environ Sci Pollut Res 28:1–14

Zhang Z et al (2016a) A novel approach of chemical mechanical polishing using environment-friendly slurry for mercury cadmium telluride semiconductors. Sci Rep 6:22466

Zhang Z et al (2016b) A novel approach of chemical mechanical polishing for cadmium zinc telluride wafers. Sci Rep 6:26891

Zhang Z et al (2018) A novel approach of chemical mechanical polishing for a titanium alloy using an environment-friendly slurry. Appl Surf Sci 427:409–415

Zhang S et al (2020a) Oxygen vacancies engineering in TiO2 homojunction/ZnFe-LDH for enhanced photoelectrochemical water oxidation. Chem Eng J 2020:125101

Zhang R, Ai Y, Lu Z (2020b) Application of multifunctional layered double hydroxides for removing environmental pollutants: recent experimental and theoretical progress. J Environ Chem Eng 2020:103908

Zhu S et al (2014) High adsorption capacity for dye removal by CuZn hydroxyl double salts. Environ Sci Nano 1(2):172–180

Zubair M et al (2018) Starch-NiFe-layered double hydroxide composites: efficient removal of methyl orange from aqueous phase. J Mol Liq 249:254–264

Publisher's Note Springer Nature remains neutral with regard to jurisdictional claims in published maps and institutional affiliations.